LAWRENCE
LIVERMORE
NATIONAL
LABORATORY

LLNL-PROC-421067

An Experimental and Kinetic Modeling Study of Methyl Decanoate Combustion

S. M. Sarathy, M. J. Thomson, W. J. Pitz, T. Lu

December 7, 2009

33rd International Symposium on Combustion
Beijing, China
August 1, 2010 through August 6, 2010

Disclaimer

An Experimental and Kinetic Modeling Study of Methyl Decanoate Combustion

S.M. Sarathy[a], M.J. Thomson[a], W.J. Pitz[b], T. Lu[c]

[a] *Department of Mechanical and Industrial Engineering, University of Toronto*
[b] *Physical and Life Sciences Directorate, Lawrence Livermore National Laboratory*
[c] *Department of Mechanical Engineering, University of Connecticut*

Abstract

Biodiesel is a mixture of long chain fatty acid methyl esters derived from fats and oils. This research study presents opposed-flow diffusion flame data for one large fatty acid methyl ester, methyl decanoate, and uses the experiments to validate an improved skeletal mechanism consisting of 648 species and 2998 reactions. The results indicate that methyl decanoate is consumed via abstraction of hydrogen atoms to produce fuel radicals, which lead to the production of alkenes. The ester moiety in methyl decanoate leads to the formation of low molecular weight oxygenated compounds such as carbon monoxide, formaldehyde, and ketene.

Key words: methyl decanoate, skeletal mechanism, biodiesel, combustion, chemical kinetic model

1. Introduction

Real biodiesel is a complex mixture of fatty acid methyl esters (FAME) with differing chain lengths and degrees of unsaturation, so it is much simpler to study the combustion chemistry of pure FAME. In order to simplify models and experiments, surrogate fuels with shorter chain lengths are chosen for biodiesel combustion chemistry studies.

A number of studies have been conducted to study the combustion of methyl butanoate (MB), and some notable ones are [1–3]. Experimental and modeling studies have also been conducted on methyl *trans*-2-butenoate (MC) [4, 5] and ethyl propanoate [6, 7]. The studies revealed that small esters are a good surrogate fuel for representing the thermochemistry of saturated long chain FAME, but they are not suitable surrogates for understanding the low temperature reactivity and autoignition properties of biodiesel. However, blends of *n*-heptane plus MB have been used to simulate combustion in engines [8, 9].

Recently, the research focus has shifted to longer chain esters. Experimental and modeling studies of methyl hexanoate [10] and methyl heptanoate [11] in a jet stirred reactor (JSR) have been performed. Zhang et al. have presented motored engine experimental data of methyl heptanoate [12] and various C_9 FAME [13].

Dagaut et al. [14] studied the oxidation of rapeseed oil methyl ester (RME) in a JSR at various temperatures and pressures. A detailed chemical kinetic mechanism for *n*-hexadecane gave a good description of the RME experimental results, with a good agreement for RME reactivity and the relative importance of C_2-C_6 alkenes.

Herbinet et al. [15] developed a detailed chemical kinetic mechanism for methyl decanoate (MD) consisting of 3012 species and 8820 reactions. The MD mechanism reproduces early CO_2 formation observed for RME in the JSR [14], a behaviour that the *n*-hexadecane model by Dagaut et al. could not reproduce. The large size of this mechanism requires enormous computing resources when attempting to model combustion in some configurations (e.g., laminar flames).

Seshadri et al. used the direct relation graph (DRG) method to reduce the detailed mechanism to a skeletal mechanism consisting of 713 elementary reactions and 125 species [16]. The skeletal mechanism predicts experimental extinction and ignition of MD in an opposed-flow diffusion flame. Their results indicate that low temperature chemistry is of minor importance in an opposed-flow diffusion flame.

The existing detailed MD mechanism [15] and the skeletal mechanism [16] have not been validated against fundamental flame structure data for MD because such experiments have not been performed. This study presents new experimental temperature and species concentration profiles for an MD opposed-flow diffusion flame, and uses this data to validate an improved skeletal mechanism for MD combustion.

2. Experimental Methods

A detailed explanation of the experimental opposed-flow diffusion flame and corresponding sampling setup has been described by Sarathy et al. [17]. A fuel mixture of 98.2% N_2 and 1.8% fuel (99% pure MD) is fed through the bottom port at a mass flux of 0.0142 g/cm^2-sec, while an oxidizer mixture of 42.25% O_2 and 57.75% N_2 is fed through the top port at a mass flux of 0.0137 g/cm^2-sec. At these plug flow conditions, the Reynold's Number is in the laminar flow regime (i.e. $Re < 400$), the flame is on the fuel side of the stagnation plane, and the fuel side strain rate is approximately 31 s^{-1}. An ultrasonic atomizer sprays the liquid fuel into a stream of N_2 gas. The temperatures of the gases exiting the top and bottom burner ports were 420 K and 400K , respectively.

Analytical techniques used to measure the species in the sample included: non-dispersive infrared detection (NDIR) for CO and CO_2; gas chromatography/flame ionization detection (GC/FID) with an HP-Al/S PLOT column for C_1 to C_5 hydrocarbons; and GC/FID equipped with a methanizer (i.e., Ni catalyst) and Poraplot-U column for oxygenated hydrocarbons such as acetaldehyde/ethenol, formaldehyde, and acrolein. The precision of species measurements is estimated to be ± 15%. Temperature measurements were obtained using a 254 μm diameter wire R-type thermocouple (Pt-Pt/13% Rh) in an apparatus similar to that used by McEnally et al. [18]. The measured temperatures were corrected for radiation losses.

3. Computational Methods

The kinetic modeling for MD oxidation in the opposed-flow diffusion flame was performed using the OPPDIF code within the CHEMKIN package [19]. The inputs to each simulation include a detailed chemical kinetic reaction mechanism, a dataset of thermochemical properties, and a dataset of transport properties.

The chemical kinetic mechanism developed here is an extension of the previously published detailed [15] and skeletal [16] mechanisms for MD. The large size of the detailed mechanism makes it impractical for use in the one-dimensional flame code (i.e., OPPDIF), while the skeletal mechanism does not contain enough species and reactions to accurately predict many species concentration profiles in the opposed-flow diffusion flame to be studied in the following. Therefore, the present study develops an intermediate sized mechanism, which balances computational performance and chemical fidelity. First, several modifications were made to the detailed chemical kinetic mechanism to better predict MD combustion, and then this modified mechanism was reduced using the DRG method.

3.1. Detailed Mechanism

Herbinet et al.'s detailed chemical kinetic mechanism [15] includes low temperature chemistry to simulate fuel ignition with NTC behaviour, as well as intermediate and high temperature chemistry to simulate fuel

combustion and product species formation. Low temperature chemistry is not addressed here because the consumption of fuel in an opposed-flow diffusion flame is dominated by high temperature chemical reactions.

For the most part, the high temperature consumption of MD proceeds similarly to a straight-chain alkane. The decomposition is driven by unimolecular decomposition and H-atom abstraction reactions leading to alkyl and alkyl-ester radicals. These radicals then react via isomerization, decomposition (e.g., *beta*-scission) and bimolecular reactions with O_2. The reader is referred to the original article [15] for further details on the detailed mechanism.

The following modifications were made to better represent the combustion of MD in the opposed-flow diffusion flame:

Herbinet et al. [20] reported an error in their mechanism [15] for the activation energy for H-atom abstractions reactions by OH from secondary C-H bonds, so this was corrected in the present mechanism.

The recombination rate of 1-octene (C_8H_{16}) and the ME2J radical to form the MD4J radical was changed to 8.80E3 $\cdot$ $T^{2.48}$ $\cdot$ exp(-6130cal/R$\cdot$T) to make it consistent with rates of analogous reactions for the MB5J, MB6J, MB7J, etc. radicals.

The recombination rate of methyl 2-propenoate (MP2D) and the 1-heptyl radical (C_7H_{15}) to form the MD2J radical was changed to 1.76E4 $\cdot$ $T^{2.48}$ $\cdot$ exp(-8130cal/R$\cdot$T) based on the rate expression given by Curran et al. [21] for the recombination of propene (C_3H_6) and the methyl radical (CH_3) to form the 2-butyl radical (sC_4H_9). Curran's estimate was modified by 2 kcal/mol to account for resonance stabilization effects of the carbonyl group in MD2J [3].

Hydrogen (H) atoms bonded to the alpha carbon in MD have bond dissociation energies (BDE) similar to tertiary C-H bonds in alkanes [3]. Therefore, H atom abstraction rates by the radicals H, OH, CH_3, CH_3O, and HO_2 were changed to analogous rates for tertiary H atom abstraction in isobutane (iC_4H_{10}). The rates for isobutane from Healy et al. [22] were multiplied by 2 to account for greater number of H atoms in the MD2J radical.

Figure 1 displays JSR simulations using various FAME and alkane mechanisms at ϕ=1.0, P=1013 kPa, τ=1 s, 0.1% fuel mole fraction. *n*-Decane simulations [23] and experimental data [24] match well, with both showing cool flame reactivity in the range of 600-800 K. Simulations using Dooley's MB mechanism [3] and Seshadri's skeletal MD mechanism [16] indicate that these models lack cool flame behaviour, and therefore they are not suitable for modeling real biodiesel low temperature chemistry.

It is observed that Herbinet's detailed MD mechanism [15] displays cool flame reactivity, but when compared to simulations for *n*-decane [23], the MD model appears to overpredict the fuel's reactivity. One would expect the reactivity of MD and *n*-decane in the JSR to be similar since both contain C_{10} alkyl chains, and shock tube studies also indicate that their reactivity is similar [15]. This model behavior was due to incorrect activation energies for H atom abstractions reactions by OH from secondary C-H bonds, as mentioned previously. After correcting these values, the modified detailed MD mechanism well predicts the

reactivity of *n*-decane.

3.2. Skeletal Mechanism

The supplemental Figure S1 compares the skeletal MD mechanism of Seshadri et al. [16], the detailed MD mechanism by Herbinet et al. [15], and experimental data for RME in a JSR [14]. The 125 species mechanism by Seshadri et al. poorly predicts the concentrations of carbon dioxide, carbon monoxide, and methane, especially at lower temperatures. This indicates that the mechanism lacks chemical fidelity when compared to the detailed mechanism.

In this study, the DRG method is used to generate a skeletal version of the modified detailed MD mechanism. The DRG methodology and its applicability to various hydrocarbon mechanisms is available in the literature [25, 26]. In order to improve the DRG method, the sample space was chosen as follows:

- combustion in a homogeneous gas phase plug flow reactor at 101.3 kPa and 1013 kPa, 900-1800 K, ϕ=0.25-2.0, with mixtures of both undiluted fuel and diluted fuel (i.e. 2% MD, 98% N_2) plus air. These conditions were simulated using the SENKIN code in CHEMKIN

- combustion in a perfectly stirred reactor (PSR) at 101.3 kPa and 1013 kPa, 900-1500 K, ϕ=0.25-2.0, τ=0.0001-1 s, and mixtures of undiluted fuel plus air. These conditions were simulated using the PSR code in CHEMKIN.

The directed graph generated from the above sampling points was used to generate a skeletal mechanism consisting of 648 species and 2998 reactions. This skeletal mechanism accurately reproduces the low temperature reactivity predicted by the detailed mechanism, as shown in Figure 1. In addition, there is a good agreement between the new skeletal mechanism and Herbinet's detailed mechanism [15] for predicted species profiles of RME in the JSR, as shown in the supplemental Figure S1. This indicates that the proposed skeletal mechanism is acceptable for modeling detailed chemical kinetic processes in the JSR. Furthermore, it is suitable replacement to the detailed mechanism for predicting the combustion properties of MD.

3.3. Thermochemical Data

The thermochemical data for MD published by Herbinet et al. [15] was used in this study. The thermochemical properties for molecules and radicals were calculated using THERM [27]. It was found that the BD groups used in the calculation of thermochemical properties for the radicals of methyl ethanoate (ME), ME2J and MEMJ, were inaccurate in the original work [15]. They were hence supdated based on bond energies calculated by El-Nahas et al. [28]. The new thermochemical parameters make these molecules more stable and decrease their decomposition rates.

3.4. Transport Properties

The transport property database was mostly from [16]. Additional transport parameters were determined for stable C_2-C_{10} saturated and unsaturated methyl esters and their corresponding radicals. We assumed

that the transport properties are similar for saturated and unsaturated methyl esters of the same chain length. For methyl ester radical species, the transport properties of their stable counterpart were used.

This study used the correlations described in [29], to calculate the Lennard-Jones collision diameter and potential well depth using the P_c, T_c, and T_b of the species. These values were obtained from [30] for C_2-C_6 methyl esters. A strong correlation exists between carbon chain length and P_c and T_c for C_3-C_6 methyl esters, as shown in the supplemental Figure S2, so we extrapolated these values for larger methyl esters using a power law function.

Experimentally measured dipole moments [31] for C_3-C_6 methyl esters fall in the range of 1.61-1.76 Debyes, so a dipole moment of 1.70 Debyes was used for the C_7-C_{10} methyl esters. Experimentally measured values for polarizability (α) were obtained from [32]. The polarizability can also be determined using the empirical relation proposed in [33]. The supplemental Table S1 presents experimentally and empirically determined polarizabilities for FAME. The calculated values are within $\pm 1\%$ of the measured values for C_3-C_6 methyl esters, so we are confident in the calculated polarizabilities for C_7-C_{10} methyl esters.

4. Results and Discussion

4.1. Opposed-Flow Diffusion Flame

The proposed skeletal MD mechanism was validated against experimental data obtained in an MD opposed-flow diffusion flame. The measured species included methyl decanoate (MD), carbon monoxide (CO), carbon dioxide (CO_2), formaldehyde (CH_2O), methane (CH_4), acetylene (C_2H_2), ethylene (C_2H_4), ethane (C_2H_6), ketene (CH_2CO), propane (C_3H_8), propene (C_3H_6), propyne (pC_3H_4), 1-butene (1-C_4H_8), 1,3-butadiene (1,3-C_4H_6), 1-pentene (1-C_5H_{10}), 1-hexene (1-C_6H_{12}), 1-heptene (C_7H_{14}), and 1-octene (1-C_8H_{16}). A species profile was identified for C_2H_4O, but we are unable to determine if the compound is ethanal (i.e., acetaldehyde) (CH_3CHO) or ethenol (C_2H_3OH) since both have the same retention time on the GC column. In addition, ethenol rapidly tautomerizes to acetaldehyde upon contact with surfaces [34], so we assume that the C_2H_4O measured in the GC is the combined concentration of acetaldehyde and ethenol in the flame. Species below the experimental limit of detection (LOD) (i.e., 5 ppm) included 1-butyne, *n*-butane, 2-butyne, *trans*-2-butene, *cis*-2-butene, pentane, hexane, propanal, 2-propenal (i.e., acrolein), 2-propanone (i.e., acetone), butanal, methyl 2-propenoate, methyl 3-butenoate, methyl 4-pentenoate, and methyl 5-hexenoate.

4.2. Temperature, Fuel, and Hydrocarbon Species

Figure 2 displays the measured and predicted species and temperature profiles obtained in the opposed-flow diffusion flame. The model reproduces the experimentally measured temperature profile very well. The reactivity of MD is also well predicted by the model. The maximum concentration of CO_2 is underpredicted by approximately 0.3%, while the maximum concentration of CO is underpredicted by approximately 0.1%.

The model well reproduces the shape of the experimental profiles and the height and position of maximum measured concentrations. In the following discussion, the model's quantitative prediction is considered good if the predicted maximum mole fraction is within a factor 1.5 of the measured maximum mole fraction. The model performs well in predicting the maximum concentrations of CH_4, C_2H_6, C_3H_4, C_3H_6, 1-C_4H_8, C_8H_{16}, C_5H_{10}, C_6H_{12}, C_7H_{14}, CH2CO, and 1,3-C_4H_6. The model moderately underpredicts (i.e., 1.5-2 times) the maximum concentration of C_2H_4 and overpredicts the concentration of C_2H_2. Both model and the experimental data indicate that the concentration of 1-alkenes decreases with increasing carbon number.

A reaction path analysis was performed for MD at 1033 K, the temperature at which approximately 50% of the fuel is consumed. Approximately 97% of the fuel is consumed via H atom abstraction by H atoms (58%), OH radicals (4%), and CH_3 radicals (28%). Abstraction is favoured for H atoms bonded to the α carbon (19%) and the other secondary carbons in the alkyl chain (10% each).

As shown in the supplemental Figure S4, the MD2J radical undergoes β-scission (99%) to form a 1-heptyl radical and methyl 2-propenoate. The 1-heptyl radical eventually leads to the formation of ethylene, 1-pentene, 1-butene, and the radicals C_3H_7 and C_2H_5.

Approximately 70% of the fuel is consumed via abstraction of H atoms from the #3 through #9 carbon atoms. An example of the subsequent reaction pathways is shown in the supplemental Figure S5 for the MD4J radical. The radicals decompose via two routes, one leading to an alkene and a methyl ester radical, and the other forming an unsaturated methyl ester and an alkyl radical. The alkyl radicals eventually result in the formation of 1-alkenes. The model predicts that the unsaturated methyl esters are consumed mainly by unimolecular decomposition to form an allyl radical and a saturated methyl ester radical that is three carbon atoms shorter (e.g., methyl 6-heptenoate decomposes to the radical methyl $\dot{4}$-butanoate, methyl 7-octenoate decomposes to the radical methyl $\dot{4}$-pentanoate, etc.). These methyl ester radicals with the radical site on the terminal carbon undergo β-scission to form ethylene and smaller methyl ester radicals. The process continues until the radical site nears the carbonyl group and the radical decomposes to a low molecular weight oxygenated species.

4.3. Oxygenated Species

Table 1 presents the maximum predicted and measured mole fractions of several unsaturated methyl esters, aldehydes, enals, ketones, ketenes, and enols. The measured and predicted concentrations of oxygenated product species can add insight into the role of the ester moiety during combustion. The following is a discussion of several important oxygenated species and their chemistry in the flame.

The model performs well at predicting the maximum concentrations of ketene (CH_2CO), but overpredicts the maximum concentrations of formaldehyde (CH_2O) and underpredicts acetaldehyde + ethenol (C_2H_4O). This is the first time ketene concentrations have been measured in combustion studies of FAME. Ketene is formed when the methyl ester radical, ME2J, undergoes β-scission to form ketene and methoxy radical

(CH_3O).

The maximum predicted concentration of CH_2O is nearly 4 times greater than the measured concentration. This discrepancy can be attributed to either experimental errors or modeling inaccuracies, so both are discussed here. The experimental measurements for formaldehyde were performed using a GC/FID equipped with a methanizer. This method for detecting formaldehyde has yielded good results in JSR studies of FAME [2, 5, 10, 11]. However, extractive sampling measurements in flames [2, 5, 35, 36] have yielded similar discrepancies between measured and predicted formaldehyde, and it was suggested in [36] that formaldehyde may be lost due to polymerization in the sampling lines.

Approximately 86% of formaldehyde is formed via the decomposition of various methyl ester radicals with a radical on the methoxy site. The current rate estimate for the decomposition of these radicals to formaldehyde are rough estimates, so detailed studies may reveal better rate constants.

The major discrepancy between the model and experiments is for unsaturated methyl ester species. The experiments did not measure detectable levels of any unsaturated methyl esters, but microliter injections of these unsaturated FAME verified that the analytical instrument used in this study was suitable for their detection. It should be noted that unsaturated methyl esters have been measured in other experimental studies of FAMEs [10–13, 37], albeit at low concentrations.

Methyl 2-propenoate (i.e., MP2D) is the unsaturated FAME predicted in the highest concentration. The supplemental Figure S6 inidcates that 94% of the MP2D is formed via β-scission of various methyl ester radicals with a radical site on the α carbon (e.g., MD2J). High concentrations of methyl 2-propenoate are predicted because multiple pathways lead to various methyl ester radicals with a radical site on the α carbon, and these form methyl 2-propenoate faster than it can be consumed via H atom abstraction reactions. The rate parameters for the methyl 2-propenoate consumption have been determined based on analogies with saturated methyl ester molecules and unsaturated hydrocarbons. Fundamental rate studies may improve the predicted concentration of methyl 2-propenoate. Another explanation for the discrepancy between the model and predicted values is possible decomposition of methyl 2-propenoate upon contact with hot surfaces in the high pressure side of the sampling line. It is possible that FAME are reacting in the sampling line to form acetaldehyde+ethenol compounds which were measured in appreciable quantities, but not predicted to be significant by the model.

4.4. Jet Stirred Reactor

The proposed skeletal mechanism for MD was also validated against experimental JSR data for RME at ϕ=1.0, P=101.325 kPa, τ=1.0 s [14]. Since MD is a smaller molecule than RME, the inlet mole fraction of MD was proportionally increased to match the inlet carbon flux of RME, as described by Herbinet et al. [15]. The comparison between the model predictions and experimental data is shown in the supplemental Figures S7 and S8.

The skeletal mechanism performs similarly to the detailed MD mechanism [15]. The concentrations of CO_2, CO, C_2H_4, O_2, CH_4, and C_3H_6 are well predicted by the skeletal mechanism. However, the concentrations of 1-C_4H_8, 1-C_5H_{10}, and 1-C_6H_{12} are overpredicted by the model, which was also observed by Herbinet et al. [15]. The prediction of alkenes does not agree with measured values because RME consists of longer chain FAME with various degrees of unsaturation, while MD is fully saturated and has a smaller chain. Although there is no data available, RME is likely to have larger carbon chains leading to the formation of larger 1-alkenes (e.g., $>C_8$) than would MD; therefore, MD over predicts the concentrations of the smaller 1-alkenes (e.g., C_4-C_6).

5. Conclusions and Recommendations

This study is the first to present experimental data for methyl decanoate combustion that can be used for validating chemical kinetic mechanisms. Of particular interest is the production of C_5-C_8 1-alkenes which are formed after β-scission of fuel radicals. The production of low molecular weight oxygenated compounds such as formaldehyde, ketene, and isomers of C_2H_4O is also observed. The experimental data presented herein was used to validate an improved skeletal mechanism for the combustion of MD. This study highlights the effectiveness of the DRG method in producing a mechanism that is computationally practical for one-dimensional flame simulations yet also retains a high level of chemical fidelity.

The proposed mechanism indicates that unsaturated methyl esters are important intermediate species in the combustion of saturated FAME. Improved rate parameters and thermochemical data for unsaturated FAME will not only improve mechanisms for saturated FAME, but they will help build comprehensive mechanisms for unsaturated FAME, such as the one recently presented by Herbinet et al. for methyl decenoates [20]

6. Acknowledgements

The portion of this work supported by LLNL was performed under the auspices of the U.S. Department of Energy by Lawrence Livermore National Laboratory under Contract DE-AC52-07NA27344. The work at University of Connecticut was supported by the National Science Foundation under Grant No. OCI-0904771.

7. Supplemental Material

This publication includes the following supplemental material:

- the proposed MD mechanism, thermochemical data, and transport data in CHEMKIN format.
- the figures and tables indicated as supplemental material in the main text.

References

[1] E. Fisher, W. Pitz, H. Curran, C. Westbrook, Proc. Combust. Inst. 28 (2000) 1579 – 1586.

[2] S. Gail, M. Thomson, S. Sarathy, S. Syed, Proc. Combust. Inst. 31 (2007) 305–311.

[3] S. Dooley, H. J. Curran, J. M. Simmie, Combust. Flame 153 (2008) 2–32.

[4] S. M. Sarathy, S. Gail, S. A. Syed, M. J. Thomson, P. Dagaut, Proc. Combust. Inst. 31 (2007) 1015–1022.

[5] S. Gail, S. M. Sarathy, M. J. Thomson, P. Dievart, P. Dagaut, Combust. Flame 155 (2008) 635–650.

[6] W. K. Metcalfe, S. Dooley, H. J. Curran, J. M. Simmie, A. M. El-Nahas, M. V. Navarro, J. Phys. Chem. A 111 (2007) 4001–4014.

[7] W. K. Metcalfe, C. Togbe, P. Dagaut, H. J. Curran, J. M. Simmie, Combust. Flame 156 (2009) 250–260.

[8] J. P. Szybist, J. McFarlane, B. G. Bunting, SAE 2007 Trans. (2007).

[9] Y. Ra, R. D. Reitz, J. Mcfarlane, C. S. Daw, SAE 2008 Trans. (2008).

[10] G. Dayma, S. Gail, P. Dagaut, Energ. Fuel 22 (2008) 1469–1479.

[11] G. Dayma, C. Togbe, P. Dagaut, Energ. Fuel 23 (2009) 4254–4268.

[12] Y. Zhang, A. L. Boehman, Combust. Flame (2009) doi:10.1016/j.combustflame.2009.09.003.

[13] Y. Zhang, Y. Yang, A. L. Boehman, Combust. Flame 156 (2009) 1202–1213.

[14] P. Dagaut, S. Gail, M. Sahasrabudhe, Proc. Combust. Inst. 31 (2007) 2955–2961.

[15] O. Herbinet, W. J. Pitz, C. K. Westbrook, Combust. Flame 154 (2008) 507–528.

[16] K. Seshadri, T. Lu, O. Herbinet, S. B. Humer, U. Niemann, W. J. Pitz, R. Seiser, C. K. Law, Proc. Combust. Inst. 32 (2009) 1067–1074.

[17] S. M. Sarathy, M. J. Thomson, C. Togbe, P. Dagaut, F. Halter, C. Mounaim-Rousselle, Combust. Flame 156 (2009) 852–864.

[18] C. McEnally, U. Koylu, L. Pfefferle, D. Rosner, Combust. Flame 109 (1997) 701–720.

[19] R. J. K. et al., Chemkin pro, 2009.

[20] O. Herbinet, W. J. Pitz, C. K. Westbrook, Combust. Flame accepted October 2009. In Press. (2009).

[21] H. Curran, Int. J. Chem. Kinet. 38 (2006) 250–275.

[22] D. Healy, H. J. Curran, J. M. Simmie, D. M. Kalitan, C. M. Zinner, A. B. Barrett, E. L. Petersen, G. Bourque, Combust. Flame 155 (2008) 441–448.

[23] C. K. Westbrook, W. J. Pitz, O. Herbinet, H. J. Curran, E. J. Silke, Combust. Flame 156 (2009) 181–199.

[24] P. Dagaut, M. Reuillon, M. Cathonnet, D. Voisin, J. Chim. Phys. PCB. 92 (1995) 47–76.

[25] T. Lu, C. Law, Proc. Combust. Inst. 30 (2005) 1333–1341.

[26] T. Lu, C. Law, Combust. Flame 146 (2006) 472–483, 2006.

[27] E. R. Ritter, J. W. Bozzelli, Int. J. Chem. Kinet. 23 (1991) 767–778.

[28] A. M. El-Nahas, M. V. Navarro, J. M. Simmie, J. W. Bozzelli, H. J. Curran, S. Dooley, W. Metcalfe, J. Phys. Chem. A 111 (2007) 3727–3739.

[29] H. Wang, M. Frenklach, Combust. Flame 96 (1994) 163–170.

[30] P. Linstrom, W. Mallard, NIST chemistry webbook, NIST standard reference database number 69, 2005.

[31] A. McClellan, Tables of Experimental Dipole Moments, Freeman, San Francisco, 1963.

[32] D. R. Lide (Ed.), CRC Handbook of Chemistry and Physics, 87th Edition, Taylor and Francis, Boca Raton, FL, 2007.

[33] R. Bosque, J. Sales, J. Chem. Inf. Comp. Sci. 42 (2002) 1154–1163.

[34] J. M. Simmie, H. J. Curran, J. Phys. Chem. A 113 (2009) 7834–7845.

[35] S. B. Dworkin, A. M. Schaffer, B. C. Connelly, M. B. Long, M. D. Smooke, M. A. Puccio, B. McAndrew, J. H. Miller, Proc. Combust. Inst. 32 (2009) 1311–1318.

[36] M. S. Kurman, R. H. Natelson, N. P. Cernansky, D. L. Miller, American Institute of Aeronautics and Astronautics (2009) 1–19.

[37] M. H. Hakka, P.-A. Glaude, O. Herbinet, F. Battin-Leclerc, COMBUSTION AND FLAME 156 (2009) 2129–2144.

List of Tables

List of Figures

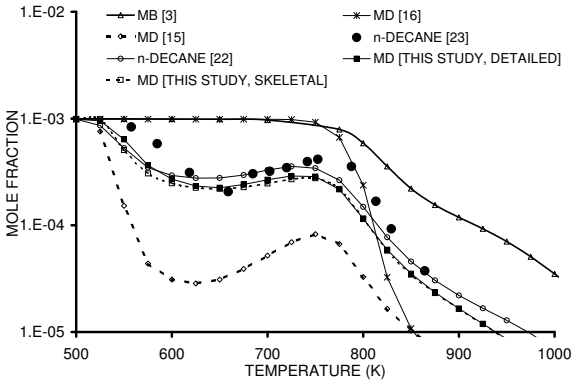

Figure 1: Experimental (symbols) and computed (lines with symbols) profiles obtained from the oxidation of methyl decanoate, *n*-decane, and methyl butanoate in a JSR at ϕ=1.0, P=1013 kPa, τ=1 s, 0.1% fuel mole fraction in O_2/N_2.

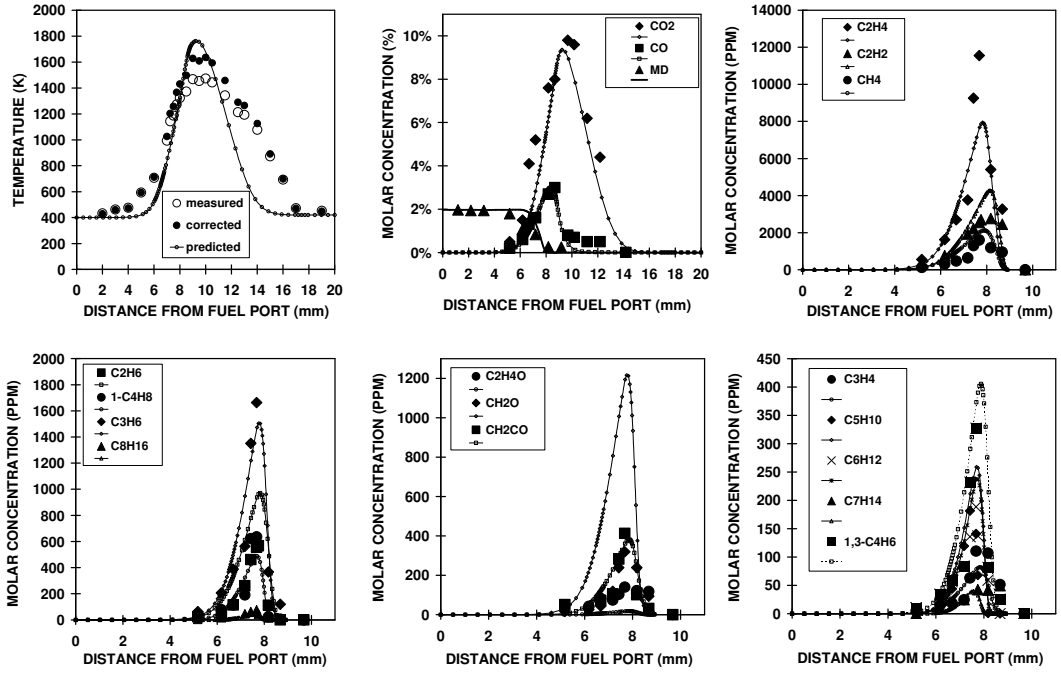

Figure 2: Experimental (solid symbols) and computed (lines with open symbols) profiles obtained from the oxidation of MD in an atmospheric opposed-flow flame (1.8% MD, 42% O_2).

Table 1: Maximum Measured and Predicted Concentration (PPM) of Oxygenated Species

	Measured	Predicted
Formaldehyde	319	1213
Ketene	413	381
Ethanal+Ethenol	100	33
Propanal	<LOD	<1
2-propenal	<LOD	32
2-propanone	<LOD	12
Methyl 2-propenoate	<LOD	939
Methyl 3-butenoate	<LOD	89
Methyl 4-pentenoate	<LOD	44
Methyl 5-hexenoate	<LOD	35

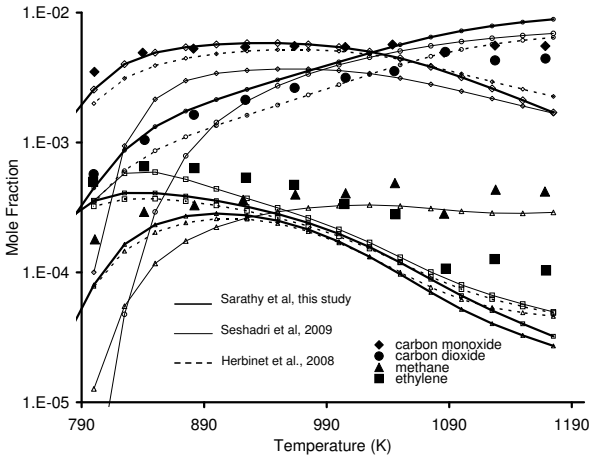

Figure S1: Comparison of MD mechanisms (lines with symbols) and experimental data (symbols) for RME in a JSR at ϕ=1.0, P=1013 kPa, τ=1.0 s [14].

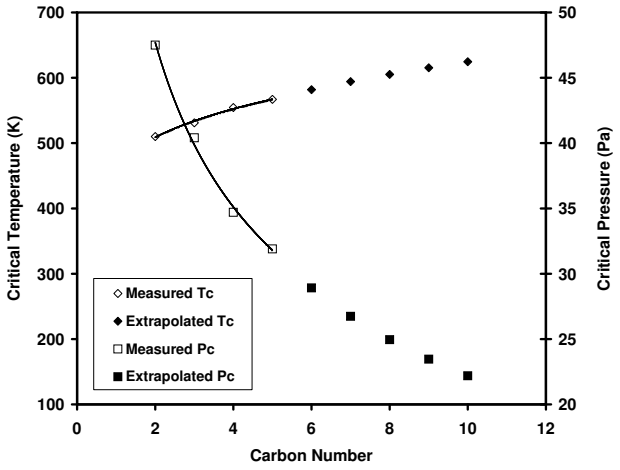

Figure S2: Critical pressure (P_c) and critical temperature (T_c) for C_2-C_{10} methyl esters.

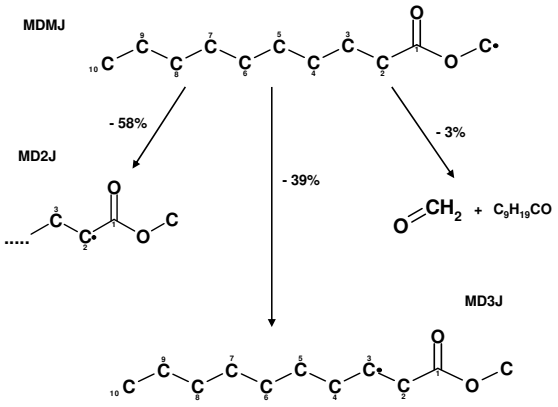

Figure S3: Reaction pathway diagram for consumption of the MDMJ radical in the opposed-flow diffusion flame at T=1040 K.

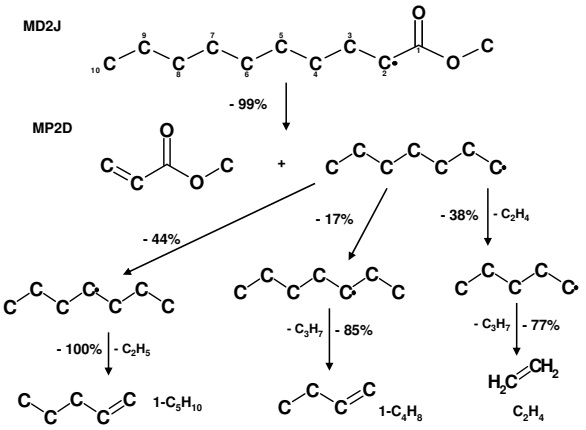

Figure S4: Reaction pathway diagram for consumption of the MD2J radical in the opposed-flow diffusion flame at T=1040 K.

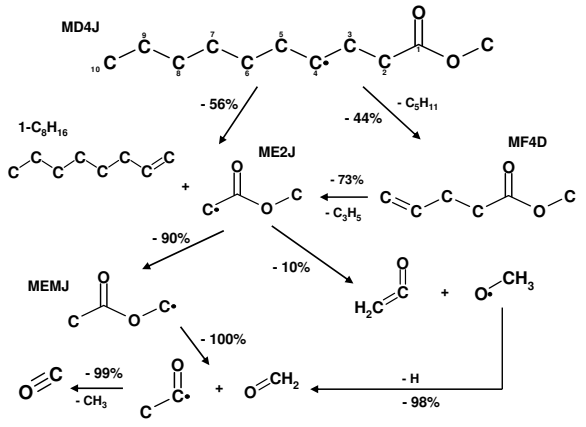

Figure S5: Reaction pathway diagram for consumption of the MD4J radical in the opposed-flow diffusion flame at T=1040 K.

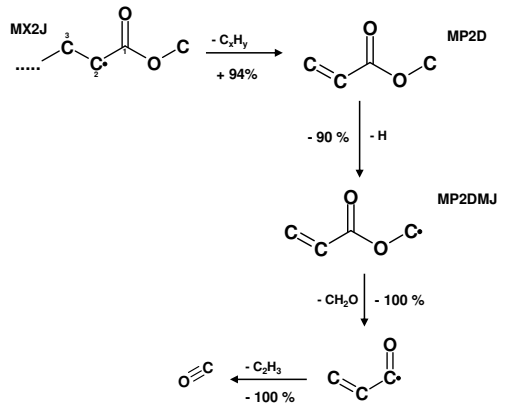

Figure S6: Reaction pathways for the formation and consumption of methyl 2-propenoate in the opposed-flow diffusion flame at T=1040 K.

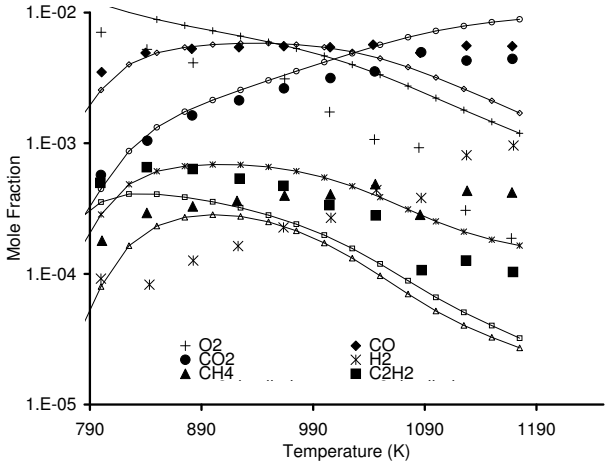

Figure S7: Comparison of proposed MD skeletal mechanism (lines with symbols) and experimental data (symbols) for RME in a JSR at ϕ=1.0, P=1013 kPa, τ=1.0 s [14].

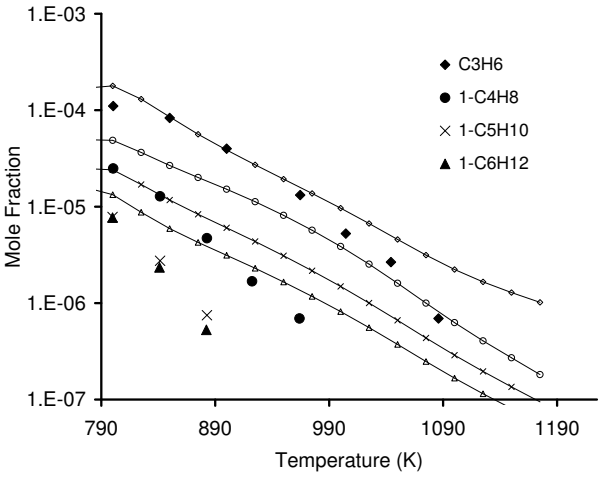

Figure S8: Comparison of proposed MD skeletal mechanism (lines with symbols) and experimental data (symbols) for RME in a JSR at ϕ=1.0, P=101.325 kPa, τ=1.0 s [14].

Table S1: Experimentally and Empirically Determined Polarizabilities (Å^3) for FAME

	Molecular Formula	Experimental [32]	Empirical [33]
Methyl ethanoate	$C_3H_6O_2$	6.94	6.89
Methyl propanoate	$C_4H_8O_2$	8.97	8.74
Methyl butanoate	$C_5H_{10}O_2$	10.41	10.59
Methyl pentanoate	$C_6H_{12}O_2$	-	12.44
Methyl hexanoate	$C_6H_{14}O_2$	-	14.29
Methyl heptanoate	$C_7H_{16}O_2$	-	16.14
Methyl octanoate	$C_8H_{18}O_2$	-	17.99
Methyl nonanoate	$C_9H_{20}O_2$	-	19.84
Methyl decanoate	$C_{10}H_{22}O_2$	-	21.69